

Optimum Location of Seismic Isolation for Manavgat Cable-Stayed Bridge

Amr Z. Elkady¹, Ahmed F. Youssef², Iman Abuelnadr³, Donovan DePeder⁴, Ayman A. Seleemah¹

¹Structural Engineering Department, Faculty of Engineering, Tanta University, Egypt.

²Structural Engineering Department, Nile Higher Institute for Engineering and Technology, Egypt.

³Seismology Department, National Research Institute of Astronomy, and Geophysics, Egypt.

⁴Bachelor of Science (B.S.), Civil Engineering, University of Illinois at Urbana-Champaign, USA.

Received: 08 Oct 2023; Received in revised form: 10 Nov 2023; Accepted: 20 Nov 2023; Available online: 30 Nov 2023

Abstract: *Seismic isolation strategies have been extensively implemented to mitigate the risk of damage in cable-stayed bridges (CSBs). The effectiveness of seismic isolation has received a great deal of attention from a number of researchers. This paper focuses on studying the seismic performance of a single pylon cable-stayed bridge with a single concave friction pendulum (SCFP) at various locations under bi-directional seismic excitations. A 3D numerical model was created using the prototype of a single pylon cable-stayed bridge located in Antalya, Turkey in order to study its seismic response. SCFP was installed at the bridge's deck-abutment, deck-pylon and pylon-foundation connection to study the reduction of the dynamic response when subjected to various seismic excitations. The efficiency of SCFP is evaluated by monitoring and controlling the displacement of the deck, acceleration, and the base of the pylon. The analytical results indicate that SCFP can effectively diminish both the base shear and the displacement of the pylon. However, the effectiveness of SCFP is significantly influenced by its location and ground motion.*

Keywords: *Seismic isolation, Single Concave Friction Pendulum (SCFP), Structure control, Cable-stayed bridges, Nonlinear dynamic analysis.*

I. INTRODUCTION

Cable-stayed bridges are renowned for their architectural appeal. They can include various cable arrangements, fan, harp, semi-fan, etc. Studies conducted on past-earthquakes damages or destruction have revealed that a bridge's behavior is mainly influenced by two factors: structural control methods and dynamic loadings (wind and earthquakes). In order to resolve these challenges, advanced strategies such as structural control approaches have emerged. These approaches can be categorized as active, semi-active, passive, and hybrid control approaches [1]. The adoption of control approaches in the structural design community has been gradual due to perceived complexity, large scale, and high costs associated with these systems. Recently, technological advancements have made control methods more practical for new bridge construction projects as well as retrofitting existing ones.

In the past three decades, many studies have focused on mitigating the structural response induced by dynamic effects. This led to the development and implementation of various structural control concepts [2]. Ali and Abdel-Ghaffar [3,4] conducted initial studies focused on utilizing isolation techniques to enhance the seismic behavior of cable-stayed bridges. Constantinou et al. [5,6] performed experimental evaluations on a seismic isolation system for cable-stayed bridges. This system comprised of multi-directional Teflon bearings, which served to account for thermal shifts and provided isolation. Additionally, control devices served the dual purpose of both restoring the bridge under seismic excitation and, offering energy dissipation capacity and structural rigidity for service loading. The seismic behavior of cable-stayed bridges was examined by Iemura and Padrono [7] using a combination of elastomeric and hysteretic bearings. This isolation strategy included both passive and semi-

active dampers to enhance seismic response. Weselowsky and Wilson [8] studied the seismic performance of cable-stayed bridges that were isolated using Lead Rubber Bearings (LRBs), particularly focusing on their behavior during near-field earthquake events. Their findings indicated the presence of an optimal level of isolation that offers limiting displacement and reduces seismic forces during earthquakes. Casciati et al. [9] evaluated the dynamic performance of a cable-stayed bridge utilizing elastomeric LRBs. They employed fragility curves as a method to assess the bridge response. A comparison was performed by Soneji and Jangid [10] in order to analyze the effectiveness of three different systems: high-damping rubber bearings (HDRBs), Lead Rubber Bearings (LRBs), and a friction pendulum system (FPS) on isolated cable-stayed bridges. They determined the optimum levels of yield strength for LRBs and the frictional coefficient for FPS that resulted in the most significant reduction of both base shear and the maximum displacement of the bridge.

Integrating isolation techniques with dampers can improve the capacity for controlling the displacement of isolated bridges. Park et al. [11] suggested the installation of a hybrid control system for cable-stayed bridges. This system incorporated LRBs to mitigate the forces generated by earthquakes. Furthermore, fluid dampers provided additional reduction in the bridge's responses. Soneji and Jangid [12] applied an additional damping mechanism using a viscous fluid damper (VFD) to reduce the seismic response of an isolated cable-stayed bridge. This approach proved effective in controlling the maximum displacement of the isolator and limiting the base shear of towers. Ismail and Casas [13,14] conducted a study focused on the seismic behavior of a cable-stayed bridge equipped with a novel isolator for controlling the displacement, accelerations, and internal forces of a bridge. They specifically investigated the bridge's response to near-fault ground motions. Cámara and Astiz [15] investigated retrofitting solutions for cable-stayed bridges. They explored the implementation of supplemental damping devices that establish a connection between the deck and the tower in the transverse direction. Elkady et al. [16, 17] conducted a study using a Tuned Mass Damper (TMD) on a scale model of Dongshuimen Bridge to simulate the earthquake excitations and evaluate the efficiency of the TMD. To enhance the seismic response of Dongshuimen bridge, Alshaer et al. [18] investigated how a Single-Tuned Mass Damper (STMD) can improve the efficiency of cable-stayed bridges under various ground motions. Additionally, they determined the ideal value of TMD mass ratio. The safety of cable-stayed bridges during earthquakes is of paramount importance because of their long spans. However, the seismic excitations affecting these bridges may not be spatially synchronous.

Based on literature reviews and studies, base isolation has been proven as an effective and economical method for mitigating structural response and damage during earthquakes. Many full-scale bridges have different base isolation systems [19]. Sliding isolators operate on the friction principle. It is assumed that as the friction coefficient decreases, the transmission of shear also decreases [20]. The base isolation technology used in this study is the single concave friction pendulum (SCFP).

SCFP bearings have been studied since 1990 [21-23]. SCFP is mainly composed of an articulated slider and a concave spherical surface. The sliding surfaces are coated with a low-friction material. Based on the pendulum function, the superstructure period is determined by the curvature radius of the SCFP bearing. Because of the concave surface, re-centering forces proportional to superstructure weight are introduced. In the last few decades, sliding bearings with adaptive seismic response have been presented [24-26]. As a response to the need for earthquake-resistant structures, several studies have been conducted to develop flexible and cost-effective isolation systems. One such system is the friction pendulum, which has garnered significant attention. In this regard, the double concave friction pendulum (DCFP) and triple concave friction pendulum (TCFP) were developed to provide enhanced seismic performance and structural stability [27-31]. For example, Tsopelas et al. [32], Kim and Yun [33], Tsai et al. [34], and Soni et al. [35] studied the effect of friction pendulum bearings on the seismic behavior of cable-stayed bridges.

The seismic behavior of a single-pylon cable-stayed bridge is significantly influenced by the method of connection between the deck and the pylon. An example of this is the Chi-Lu Bridge, a single-tower cable-stayed bridge that suffered damage during the 1999 Chi-Chi Earthquake in Taiwan [36]. Chadwell [37] performed numerical investigations aimed at evaluating the effectiveness of an isolation system designed to protect the Chi-Lu cable-stayed bridge. The collapse of the Benten Viaduct occurred during the Hanshin Earthquake in Japan in 1995. In its reconstruction, the implementation of base-isolation technology included the installation of lead rubber bearings (LRB) at the bottom of the piers [38]. Ates and Constantinou [39] conducted an examination of a curved bridge that was isolated using friction pendulum bearings positioned between the deck and the piers. Atmaca et al. [40] conducted nonlinear time history analyses to investigate the seismic behavior of the Manavgat cable-stayed bridge. The bridge was isolated using SCFP implemented between the pylon base and the foundation. Javanmardi et al. [41] studied an existing cable-stayed bridge under bi-directional seismic excitation using LRBs at the base of the pylon. Previous numerical studies primarily centered on examining the seismic behavior of cable-

stayed bridges that were isolated using sliding bearings. However, the optimal placement of bearings in single-pylon cable-stayed bridges has not been extensively explored.

The present study contains nonlinear dynamic analyses for single pylon cable-stayed bridge under bi-directional seismic excitation. The objectives of the study are to: (1) investigate the seismic performance of a single pylon cable-stayed bridge with the installation of SCFP at various locations, (2) evaluate the effectiveness of SCFP on the seismic behavior of a single pylon cable-stayed bridge; and (3)

determine the optimum location of SCFP to enhance the seismic behavior of single pylon cable-stayed bridges.

II. DESCRIPTION OF MANAVGAT BRIDGE

Manavgat bridge was constructed in 2009 in Antalya, Turkey using the balanced cantilever construction method. The total length of the bridge is 202m, and it features a lambda-shaped steel tower positioned at the mid-span of the bridge as shown in Fig.1. Fig.2 shows the general layout of Manavgat cable-stayed bridge, including typical cross-sections at various locations.



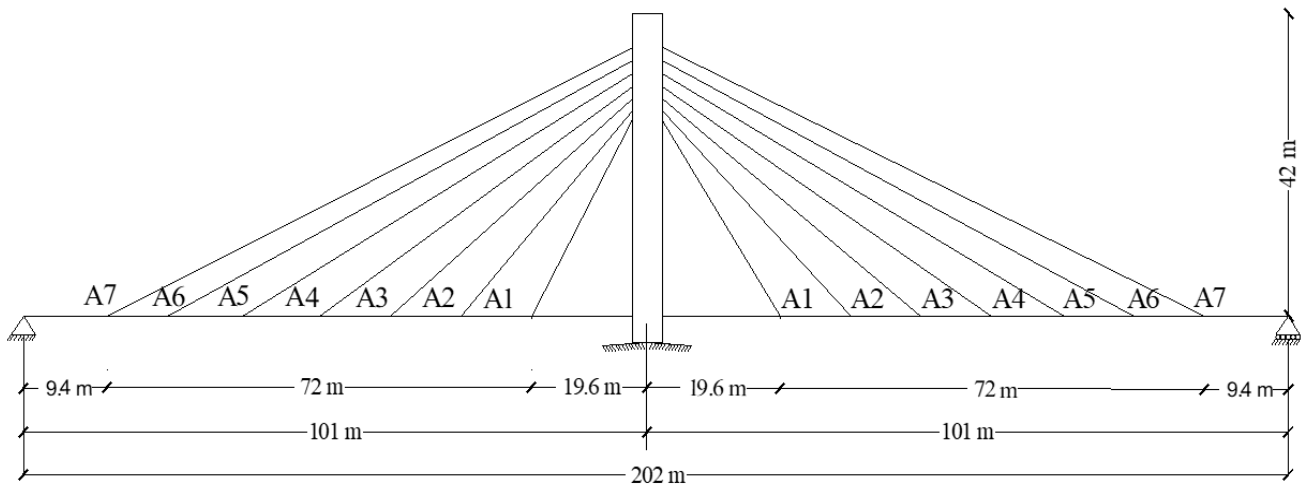
Fig. 1. Manavgat cable-stayed bridge(<https://structurae.net/en/structures/manavgat-antalya-bridge>)

The bridge has two equal spans of 101m and a width of 13.7m. It is designed to accommodate two lanes of traffic. The cross-section of the 42m steel tower is hollow and hexagonal. The bridge deck is a composite section consisting of a 25cm thick layer of concrete supported by cross girders placed at a regular spacing of 3m. Additionally, there are two main girders positioned at the outer edges of the deck with an average depth of 1.8m.

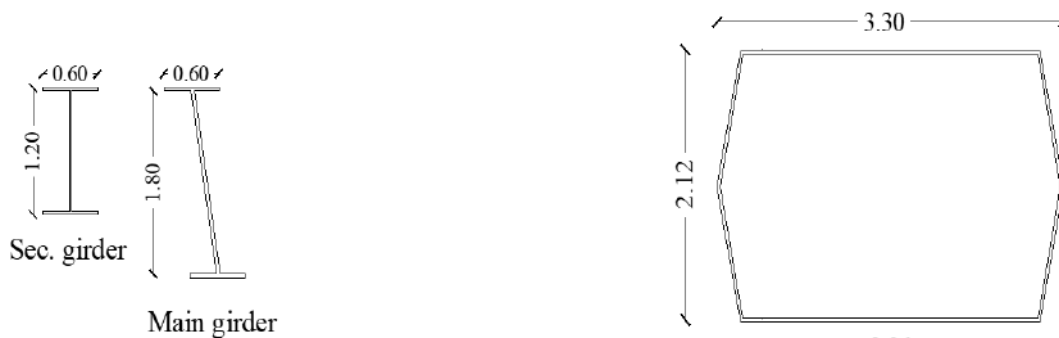
The pylon connects to 28 stay cables with a semi-fan arrangement that supports the bridge deck. The centermost cable attaches to the deck 19.6m away from the pylon, while the gap along the deck between each additional cable measures 12m. The last cable attaches to the deck 9.4m away from the shore supports [40]. It is assumed that the bridge deck is continuous from one end to the other. Tables 1,2 describe the bridge's material properties, cable properties, and general description.

Table 1. Material properties of the bridge.

Material	Unit Weight (KN/ m ³)	Strength (MPa)	Modules of Elasticity (MPa)	Poisson Ratio
Deck Concrete	25.0	40	34000	0.2
Structural Steel	78.5	450	200000	0.3
Strand	78.5	1860	197000	0.3



(a) Elevation of the bridge.



(b) Deck cross section.

(c) Pylon cross section.

Fig. 2. General layout of Manavgat cable stayed bridge (a) Elevation of the bridge; (b) Deck cross section; (c) Pylon cross section.

Table 2. Properties of the stay cables.

Cable No	No. of Strands	Approximate angle to horizontal	Diameter of Strand(mm)	Cross Section area of Stay Cable(mm ²)
A1	15	56	15.2	2100
A2	16	45	15.2	2240
A3	19	37	15.2	2660
A4	19	33	15.2	2660
A5	22	29	15.2	3080
A6	19	26	15.2	2660
A7	24	24	15.2	3360

III. ANALYTICAL MODEL OF THE BRIDGE

A finite-element model (FEM) of the bridge was developed using SAP2000 software. The model consists of 1102 beam elements, 28 truss elements, and 1980 shell elements. A beam element is used to model the pylon and steel I-beam profile (part of the deck). The deck is modeled as a four-node shell element. The cables are modeled as truss elements, capable of withstanding only tensile forces. The

support condition at the base of the pylon is fixed, preventing both rotational and translational movement. The right abutment is modeled as a roller, facilitating longitudinal movement while restricting vertical and transverse translation ($U_Y = U_Z = 0$). The left abutment is hinged, which allows the abutment to rotate around longitudinal and transverse axes without permitting any translation ($U_X = U_Y = U_Z = 0$). The FEM of the bridge is shown in Fig.3.

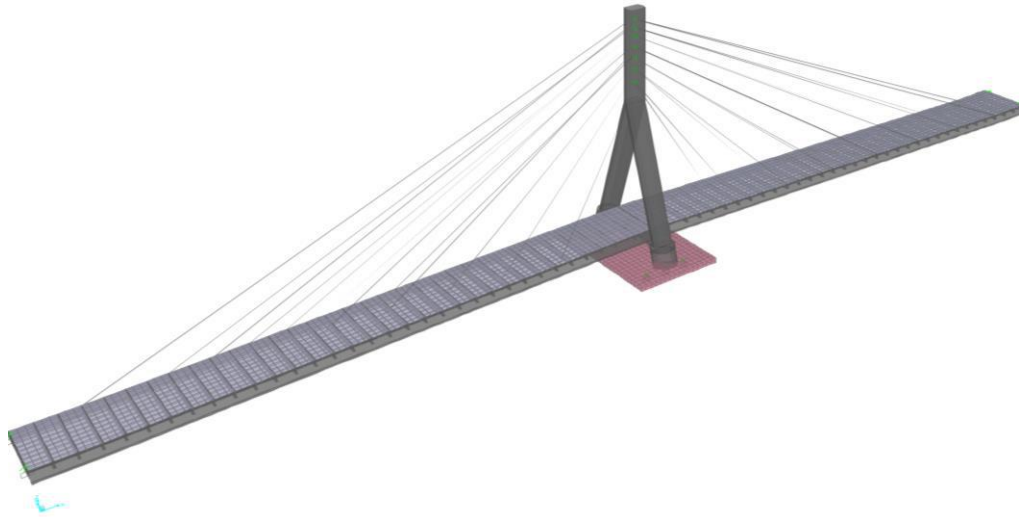


Fig. 3. FEM of the bridge.

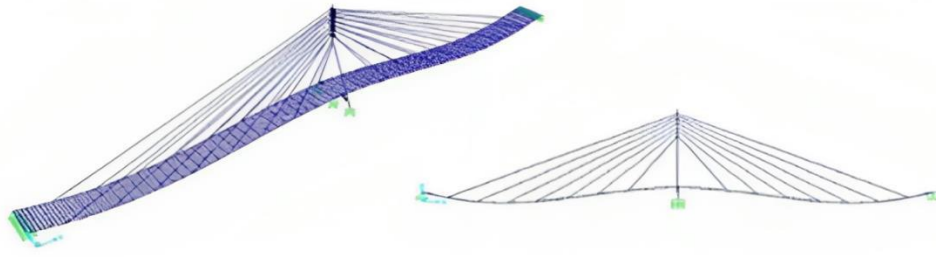
The geometric nonlinearity response of cable-stayed bridges depends on (i) large displacements (P-D effect), (ii) beam-column effect, and (iii) cable sag. [42]. It is generally recognized that the third factor takes the most significance. Numerous finite element models have been presented to account for cable behavior while taking cable sag into consideration [43-46]. One approach involves the linearization of cable stiffness by employing a modified modulus of elasticity that is lower than the actual modulus. This concept was initially introduced by Ernst and is expressed by:[47]

$$E_{modi} = \frac{E_C}{1 + \frac{(WL_x)^2(EA)_C}{12T_0^3}} \quad (1)$$

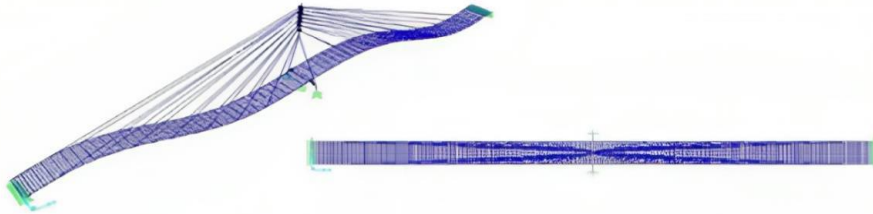
Where E_C is the modulus of elasticity of the material, L_x is the projected length in plane, A_C is the area of the cross-section, W is unit weight, and T_C is the tension in the cable. Wilson and Gravelle [48] mentioned that the equivalent modulus value is nearly identical to the actual modulus of

elasticity. Therefore, the impact of nonlinearity attributed to cable sag was disregarded within this investigation. In this study, the cables were considered to exhibit a purely linear relationship between force and deformation, described by the material modulus.

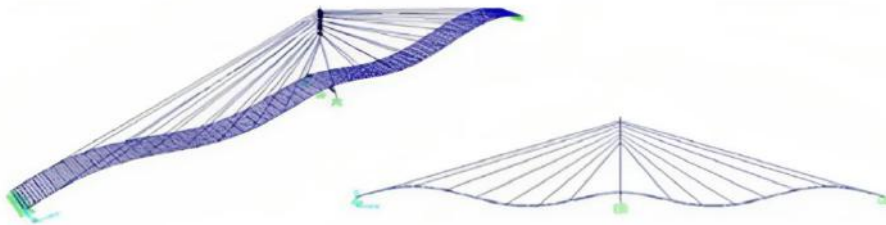
Preliminary verification was conducted to evaluate the model's ability to accurately simulate the bridge. The results were compared against prior results determined by Atmaca et al. [40]. Fig.4 illustrates the first five modes of the bridge, including longitudinal, lateral, vertical, and torsional modes. Table 3 shows a summary of the vibrational properties of the bridge, including natural periods, participating mass ratios, and a description of each mode. The first five natural periods obtained from the FEM analysis (0.831, 0.498, and, 0.436 seconds) are in agreement with the prior results (0.825, 0.536, and 0.452 seconds). It is clear that the comparison is satisfactory and represents the ability of the FEM to express the actual behavior of the Manavgat cable-stayed bridge.



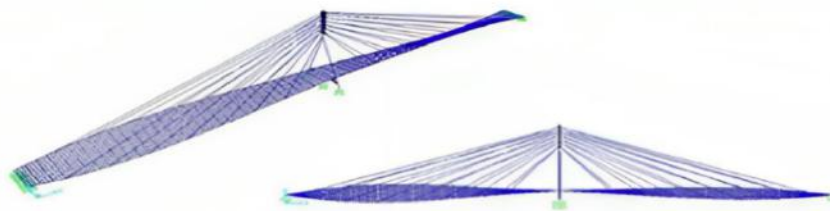
The Frist Mode (T= 0.831 Sec)



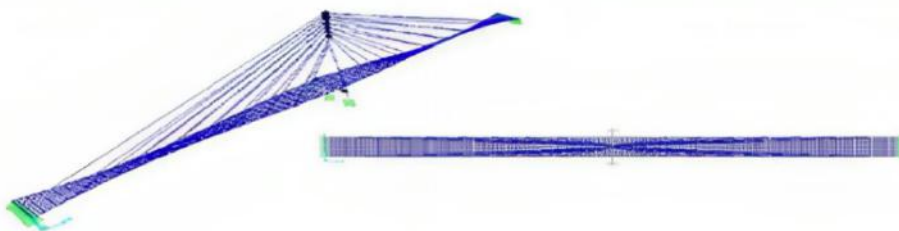
The Second Mode (T= 0.498 Sec)



The Third Mode (T= 0.436 Sec)



The Fourth Mode (T= 0.310 Sec)



The Fifth Mode (T=0.309 Sec)

Fig. 4. Analytical modes of vibration of the bridge.

Table 3. A summary of the vibration properties of the bridge.

Mode No	Period (Sec)	Modal participating mass ratios (%)							Vibration mode
		Longitudinal Direction	Longitudinal Direction (Cumulative)	Lateral Direction	Lateral Direction (Cumulative)	Vertical Direction	Vertical Direction (Cumulative)	Vertical Direction (Cumulative)	
1	0.831	0.003	0.003	0.000	0.000	0.596	0.596	0.596	1 st Vertical
2	0.498	0.001	0.003	0.000	0.000	0.000	0.000	0.596	1 st Transverse bending
3	0.436	0.000	0.003	0.000	0.000	0.031	0.031	0.627	2 nd Vertical
4	0.310	0.000	0.003	0.000	0.000	0.000	0.000	0.627	1 st Longitudinal bending
5	0.309	0.000	0.003	0.000	0.000	0.000	0.000	0.627	2 nd Longitudinal bending
6	0.280	0.000	0.003	0.000	0.000	0.000	0.000	0.627	3 rd Transverse bending
7	0.253	0.000	0.003	0.000	0.000	0.092	0.092	0.719	3 rd Vertical
8	0.231	0.000	0.003	0.000	0.000	0.000	0.000	0.719	3 rd Longitudinal bending
9	0.220	0.000	0.003	0.001	0.001	0.000	0.000	0.719	4 th Longitudinal bending
10	0.212	0.000	0.003	0.065	0.066	0.000	0.000	0.719	5 th Longitudinal bending

IV. SINGLE CONCAVE FRICTION PENDULUM

Nonlinear dynamic analysis was performed by comparing the performance of the CSB under different excitation records to select the optimum location of SCFP. Two groups

were created to use in this study; Group I SCFP is applied between the pylon and the foundation, while Group II SCFP is applied between the deck and strut attached to pylon as shown in Fig.5.

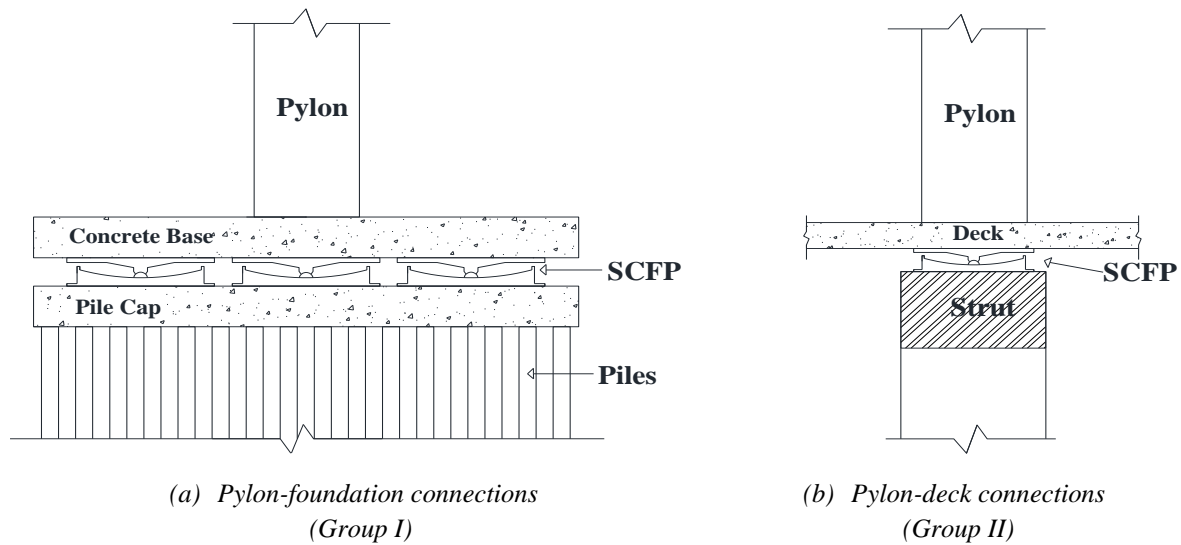


Fig. 5. Schematic of the setup proposed for SCFP.

Description of single concave friction pendulum

The SCFP system is comprised of three distinct components: the upper spherical concave surface, the lower spherical concave surface, and the articulated slider. The

articulated slider is coated with PTFE (polytetrafluoroethylene), a type of non-stick material known for its low coefficient of friction. This coating allowing for smooth sliding between the slider and concave surfaces. Fig.6 illustrates a cross-section view of the SCFP [49,50].

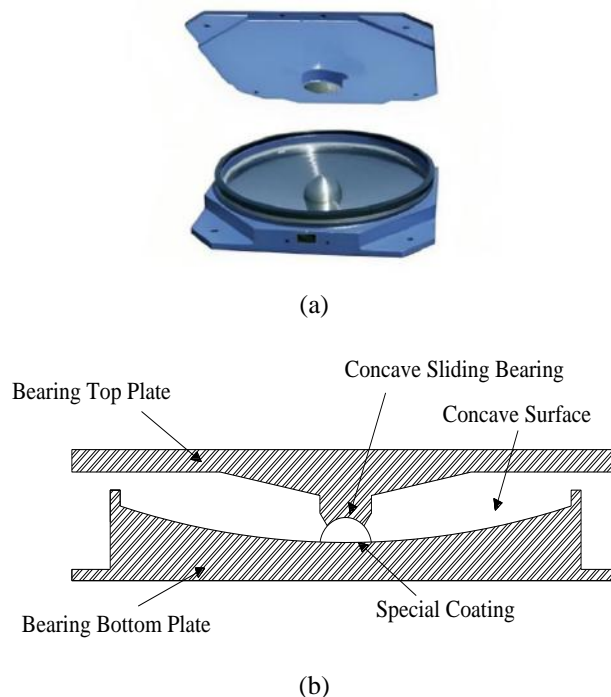


Fig. 6. Single friction pendulum bearing (SCFP) (a) three-dimensional view;(b) cross section view.

When a supported structure is excited by horizontal motion, the SCFP bearings induce a pendular trajectory. The uplift of the displaced structure serves as a restorative force due to gravity. The period of the isolated structure behaves similarly to a pendulum and remains independent of the structural mass [51]. Without considering the effects of friction, the period of a rigid structure isolated with SCFP bearings can be determined by:

$$T = 2\pi \sqrt{\frac{R}{g}} \tag{2}$$

Where R represents the radius of the sliding surface, g represents the gravitational constant. The flexibility and energy dissipation mechanisms in SCFP bearings are separate. The structure's design stiffness is determined by determining the radius of curvature of the sliding surface. The level of energy dissipation is dependent on three key design factors: the arrangement of the sliders, the level of pressure at the overlay-slider interface, and the level of concavity of the surface finish. By adjusting these factors, the desired friction coefficient is obtained.

Table 4. Various locations of single concave friction pendulums

NO	Case	Location
Group I	Case IA	Two isolators are installed at each abutment, while six isolators are located between the pylon base and the foundation.
	Case IB	Two isolators are installed at the right abutment, while six isolators are located between the pylon base and the foundation.
	Case IC	Two isolators are installed at the left abutment, while six isolators are located between the pylon base and the foundation.
	Case ID	Six isolators are located between the pylon base and the foundation only.
Group II	Case IIA	Two isolators are installed at each abutment, while three isolators are located between the deck and strut attached to the pylon.
	Case IIB	Two isolators are installed at the right abutment, while three isolators are located between the deck and strut attached to the pylon.
	Case IIC	Two isolators are installed at the left abutment, while three isolators are located between the deck and strut attached to the pylon.
	Case IID	Three isolators are located between the deck and strut attached to the pylon only.

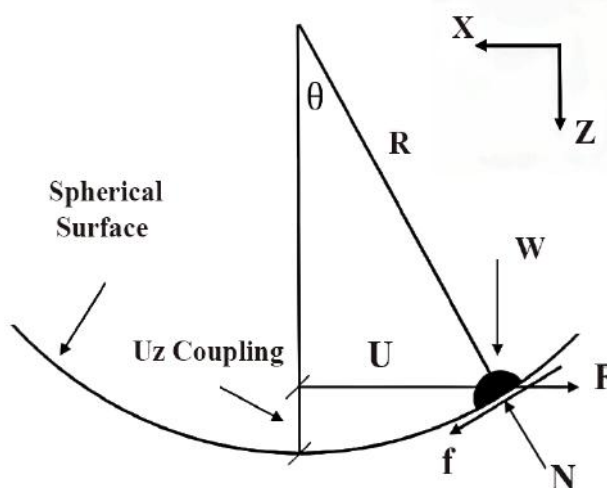


Fig.7. Forces acting on the articulated slider in SCFP bearings.

The bi-directional motion of an SCFP bearing is derived below using equilibrium equations. The SCFP bearing's resistance force is described by balancing the forces acting on the articulated slider as shown in Fig.7. The lateral force F acting at displacement u can be calculated by:

$$F = N \sin \theta + f \cos \theta \tag{3}$$

Where:

N is the normal force between the sliding surfaces;

f is the friction force at the sliding surface;

θ is the angle.

Similarly, the applied weight W can be calculated by:

$$W = N \cos \theta + f \sin \theta \tag{4}$$

The angle θ satisfies the following relationships:

$$\sin \theta = \frac{u}{R} \quad \text{and} \quad \cos \theta = \frac{\sqrt{R^2 - u^2}}{R} \tag{5}$$

Where:

u represents the displacement;

R is the radius of the spherical surface.

The friction force is commonly dependent on multiple variables, with velocity and pressure being the most influential factors [52].

In the case of Coulomb friction, the friction force (f) can be expressed as:

$$f = \mu N \tag{6}$$

The force-displacement behavior of SCFP can be described by the following equation:

$$F = N \frac{u}{R} + \mu N \operatorname{sgn}(\dot{u}) \cos \theta \tag{7}$$

$$= (W \frac{u}{R} + \mu W \cos \theta) \left(\frac{1}{\cos \theta + \mu \sin \theta} \right)$$

Where:

μ represents a constant coefficient of friction;

N is the normal force between the sliding surfaces.

$\operatorname{sgn}(\cdot)$ is the signum function used to determine the correct sign of the friction force. SCFP bearings have displacement capacities of less than 20% of R ($u/R < 0.2$), and the minimum value of $\cos \theta$ is 0.98 while the maximum value of $\sin \theta$ is 0.20. The simplified equation is as follows:

$$F = W \frac{u}{R} + \mu W \operatorname{sgn}(\dot{u}) \tag{8}$$

In the literature, it is common to express Eq. 7 in terms of N , assuming that $N \approx W$. This approximation assumes that $\cos \theta$ is approximately equal to 1.0 and that the horizontal axial load on the bearings is specified as illustrated in Fig.8.

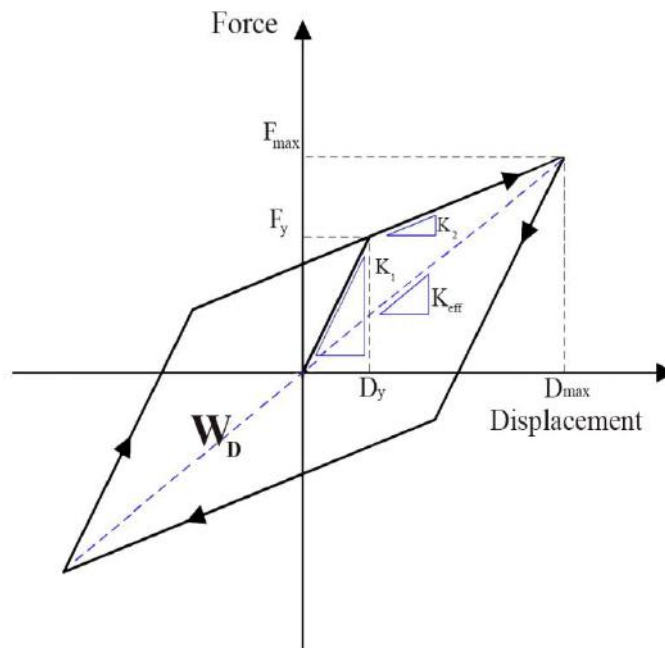


Fig.8. Idealized force-deformation relation of SCFP bearing.

Modeling of single concave friction pendulum

SAP 2000 was used to model the SCFP bearing. The bearing was selected as an isolator device, and was simulated as a direct link. Two sliding systems were considered

in this model: SCFP1 and SCFP 2. The former is a placement at the abutments, and the latter is a placement between the pylon base and foundation as shown in Table 4. The parameters of each are listed below in Table 5 [40].

Table 5. Parameters of single concave friction pendulums.

Parameters	SCFP1	SCFP2
Vertical Stiffness (Kn/m)	87964594	87964594
Effective Stiffness (Kn/m)	1014.43	10806.48
Elastic Stiffness (Kn/m)	48600	517725
Friction Coefficient Slow	0.09	0.09
Friction Coefficient Fast	0.045	0.045
Rate Parameter	50	50
Radius of sliding Surface (m)	1.4	1.4

V. SEISMIC RESPONSE ANALYSES

Selection of ground motions

In order to study the seismic response of the bridge under a strong earthquake, three ground motion models were used: ERZ-EW and ERZ-NS components of the Erzincan earthquake, BOL-000 and BOL-090 components of the

Duzce earthquake, as well as ERCIS-EW and ERCIS-NS components of the Van-Ercis earthquake. These are listed in Table 6. The ground motions for all these events were obtained from Disaster and Emergency Management Authority (AFAD) and Pacific Earthquake Engineering Research Center (PEER) [53].

Table 6. Summary of ground motions of the Analysis.

No.	Earthquake	Components	Date	PGA (g)
01	Erzincan	EW	1992	0.496g
		NS		0.515g
02	Duzce	BOL000	1999	0.728g
		BOL090		0.822g
03	Van-Erics	NS	2011	0.173g
		EW		0.182g

Equation of motion under seismic load

The equation of motion governing the three-dimensional vibration of the bridge, under seismic load can be expressed as:

$$[M][\ddot{u}] + [C][\dot{u}] + [K][u] = 0 \quad (9)$$

Where:

M Structure quality matrix;

C Structural damping matrix;

K Structural stiffness matrix;

u Node displacement vector; $u = u_s + u_g$

u_s Displacement of unsupported joints of the structure;

u_g Displacement of the structural support node.

Equation (9) can be expressed in a partition form as follows:

$$\begin{bmatrix} M_{ss} & M_{sg} \\ M_{gs} & M_{gg} \end{bmatrix} \begin{bmatrix} \ddot{u}_s \\ \ddot{u}_g \end{bmatrix} + \begin{bmatrix} C_{ss} & C_{sg} \\ C_{gs} & C_{gg} \end{bmatrix} \begin{bmatrix} \dot{u}_s \\ \dot{u}_g \end{bmatrix} + \begin{bmatrix} K_{ss} & K_{sg} \\ K_{gs} & K_{gg} \end{bmatrix} \begin{bmatrix} u_s \\ u_g \end{bmatrix} = 0 \quad (10)$$

If the unit mass matrix is replaced by the centralized mass matrix, the following is obtained:

$$\begin{bmatrix} M_{ss} & 0 \\ 0 & 0 \end{bmatrix} \begin{bmatrix} \ddot{u}_s \\ \ddot{u}_g \end{bmatrix} + \begin{bmatrix} C_{ss} & C_{sg} \\ 0 & 0 \end{bmatrix} \begin{bmatrix} \dot{u}_s \\ \dot{u}_g \end{bmatrix} + \begin{bmatrix} K_{ss} & K_{sg} \\ 0 & 0 \end{bmatrix} \begin{bmatrix} u_s \\ u_g \end{bmatrix} = 0 \quad (11)$$

Therefore,

$$M_{ss}\ddot{u}_s + C_{ss}\dot{u}_s + C_{sg}\dot{u}_g + K_{ss}u_s + K_{sg}u_g = 0 \quad (12)$$

In the seismic action of cable-stayed bridges, the node displacement can be written as:

$$M_{ss}\ddot{u}_{vs} + C_{ss}\dot{u}_{vs} + K_{ss}u_{vs} + M_{ss}\ddot{u}_{ps} + C_{ss}\dot{u}_{ps} + C_{sg}\dot{u}_{ps} - K_{ss}u_{ps} - K_{sg}u_{pg} = 0 \quad (13)$$

According to the pseudo-static displacement principle of earthquake action, it can be seen that:

$$K_{ss} u_{ps} + K_{sg} u_{pg} = 0 \quad (14)$$

The structural motion equation under earthquake is derived:

$$M_{ss} \ddot{u}_{vs} + C_{ss} \dot{u}_{vs} + K_{ss}u_{vs} + M_{ss}R\ddot{u}_{pg} = 0 \quad (15)$$

Generally, the direct integration method is used to solve the motion time history equation.

VI. RESULTS AND DISCUSSION

To evaluate the bridge's performance, the subsequent results were obtained for each analysis:

- I. Maximum vertical displacements of the deck, ($U_{z,max}$).
- II. Displacement of the top pylon in longitudinal and transverse directions, (U_x & U_y).
- III. Acceleration of the top pylon in longitudinal and transverse direction, (A_x & A_y).
- IV. Maximum pylon base shear in longitudinal and transverse directions, ($R_{x,max}$ & $R_{y,max}$).

First Group (Group I)

Deck response

The Maximum vertical displacements of the deck under seismic excitation are plotted in Fig.9. The effect of isolators is approximately similar in all isolation cases except case (ID), which has slightly higher displacements. The percentage of vertical displacement for Erzincan, Duzce, and Ercis ground motions are 40%, 18.20%, and 45.30%, respectively.

Tower response

The displacement and acceleration responses at the top of the pylon are presented in Fig.10 and Fig.11, respectively. Fig.10 shows a comparison of displacement at the top of pylon, which clearly shows similar results in most isolation cases. However, Case (ID) shows significant reduction in pylon displacement compared to other cases. Reductions in longitudinal displacement for Case ID under the Erzincan, Duzce, and Van-Erics ground motions are 77.20%, 78.50%, and 63.30% respectively. Reductions in the transverse direction are 76.92%, 54.50%, and 67.50% respectively. Fig.11 shows a comparison of acceleration at the top of the pylon. Longitudinal acceleration is approximately similar in most isolation cases. However, longitudinal acceleration for case (ID) approaches zero for the three ground motions. Transverse acceleration for case (ID) significantly increases compared to other cases with percentages of 65.30%, 68.88%, and 78.45% respectively.

Base shear

Fig.12 compares the base shear of the pylon. Case (ID) reduced its values more than the other cases in both the longitudinal and transverse direction. However, the responses of the isolated bridges in the longitudinal direction are less than the responses in the transverse direction because the isolation design has been done with specific targets set for the longitudinal direction. Case (ID)'s reductions in the longitudinal direction to levels of the response of Erzincan, Duzce, and Van-Erics ground motions are 27.20%, 62.50%, and 12.30% respectively. Reductions of the transverse direction to levels of the response of ground motions were 78.50%, 65.20%, and 16.30% respectively.

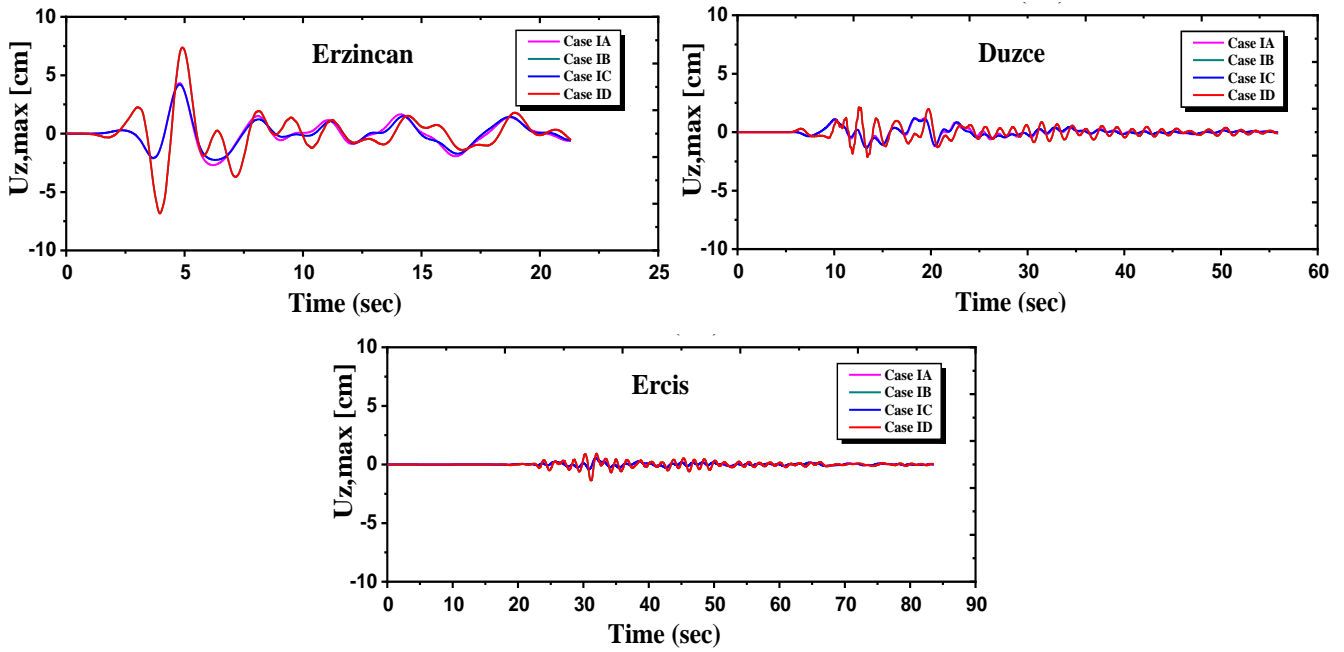
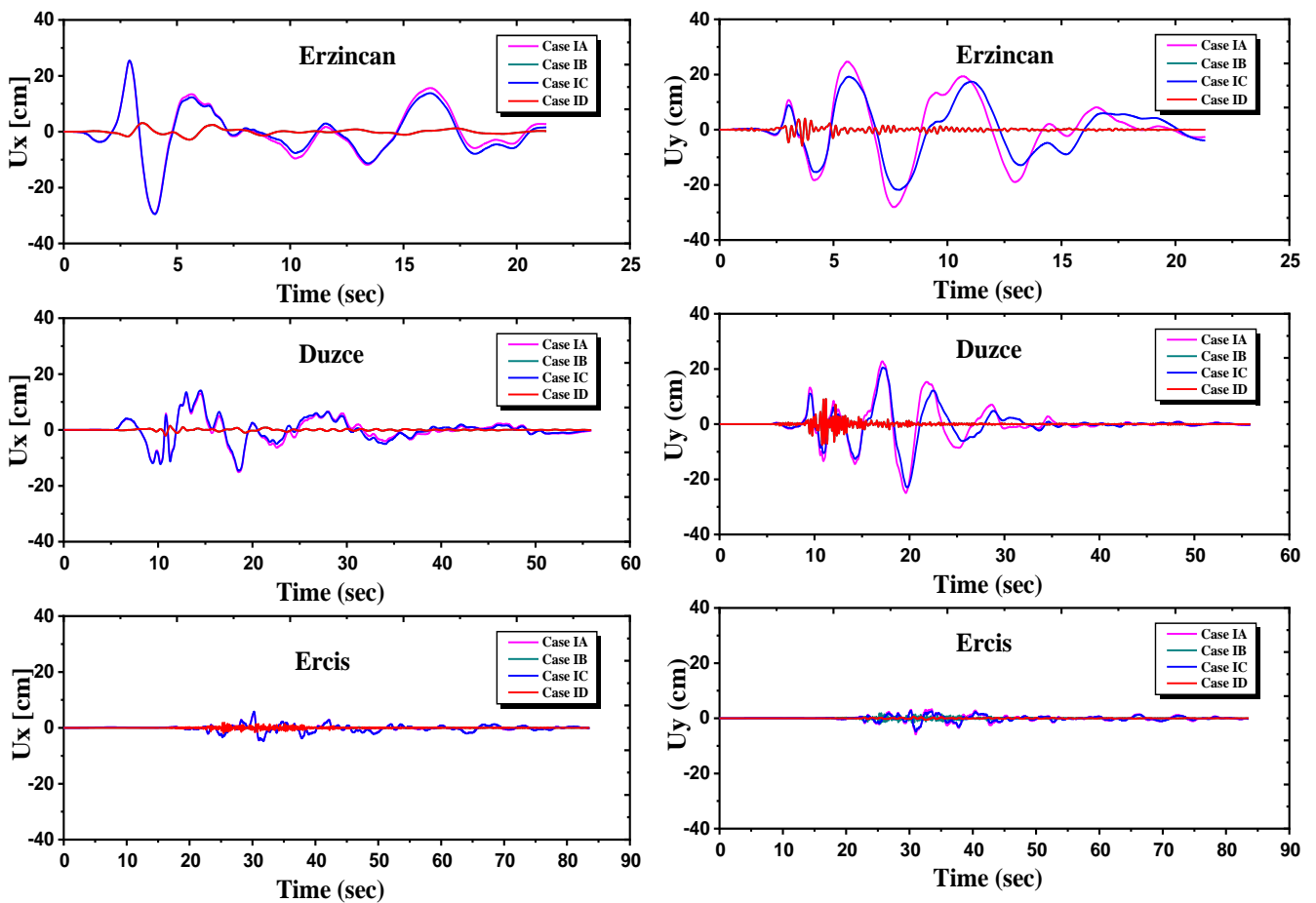


Fig. 9. Maximum vertical displacement of the deck under seismic excitations.



(a) Longitudinal Direction

(b) Transverse Direction

Fig. 10. Top pylon displacement under seismic excitations.

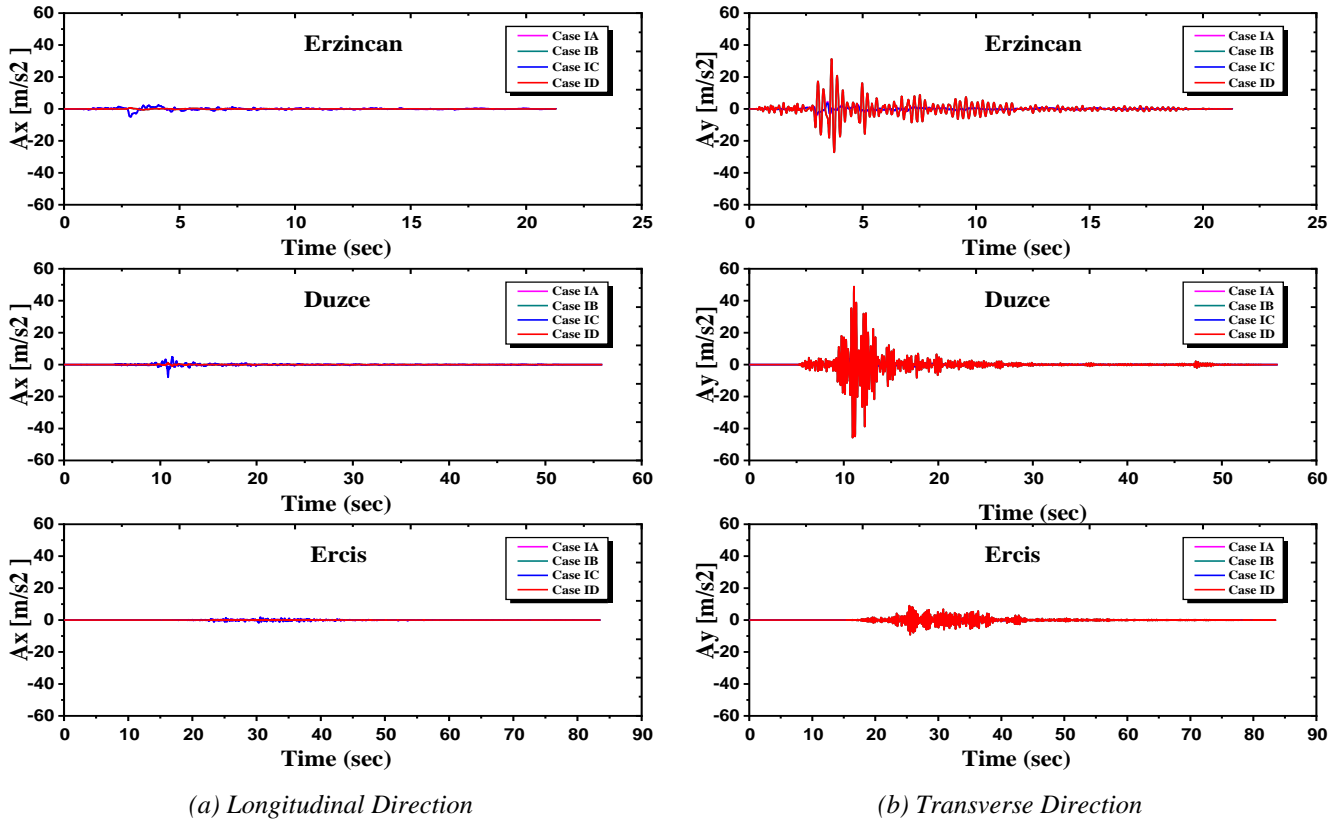


Fig. 11. Top pylon acceleration under seismic excitations

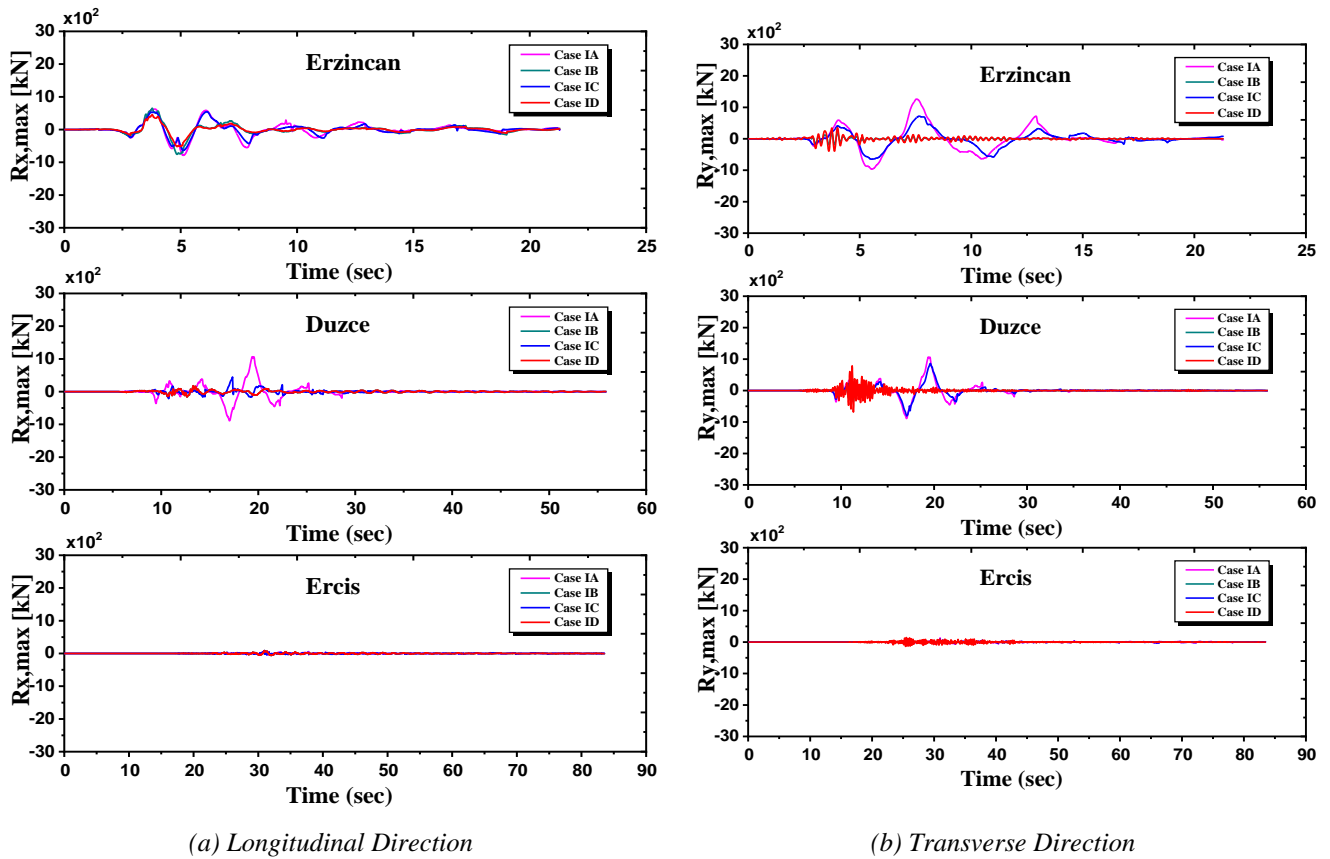


Fig. 12. Pylon base shear under seismic excitations.

Second Group (Group II)

Deck response

The Maximum vertical displacements of the deck under seismic excitation are plotted in Fig.13. The effect of isolators is approximately similar in all isolation cases except case (IID), which was comparatively more effective at reducing vertical displacements. The percentage of vertical displacements for Erzincan, Duzce, and Ercis ground motions for case IID are 68.75%, 31.81%, and 44.30%, respectively.

Tower response

The displacement and acceleration responses at the top of the pylon are presented in Figs.14,15. Fig.14 clearly shows that displacements are approximately similar in most isolation cases. However, case (IID) significantly decreases displacement compared to the other cases; longitudinal reductions in response to the Erzincan, Duzce, and Van-Erics ground motions are 90.40%, 85.71%, and 62.50% respectively. Levels of response to the various ground motions reach zero in the transverse direction, occurring between the isolated bridges. Fig.15 shows that longitudinal acceleration is approximately similar in most isolation cases. However, case (IID) has nearly zero longitudinal acceleration for the three ground motions. However, transverse acceleration for case (IID) is significantly higher than other cases with

percentages of 86.25%, 78.80%, and 46.65% for the Erzincan, Duzce, and Van-Erics ground motions respectively.

Base shear

Fig.16 compares the base shears of the pylon. Case (IID) reduced its values more than the other cases in both the longitudinal and transverse directions. However, the responses of the isolated bridges in the longitudinal direction are less than the responses in the transverse direction because the isolation design has been done with specific targets set for the longitudinal direction. Reductions of the longitudinal direction to levels of the response of Erzincan, Duzce, and Van-Erics ground motions are 37.5%,30.81%, and 10.44% respectively. Reductions of the transverse direction to levels of the response of ground motions were 78.57%, 75.20%, and 67.60% respectively.

Based on these results, it is clear that case (D) has significantly improved the seismic response of bridge more than all other isolation cases in the two groups (I&II). Allowing the end span to displace freely can lead to extensive damage due to pounding and excessive bending demands on the superstructure's strong axis.

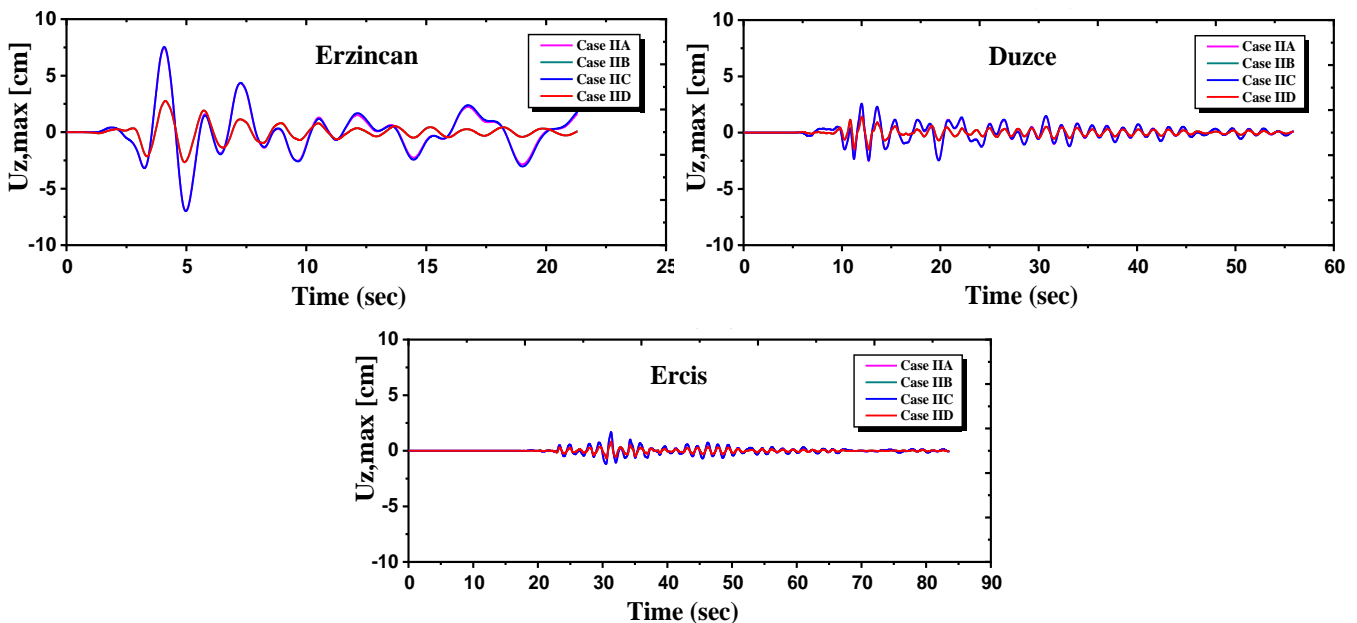


Fig. 13. Maximum vertical displacement of the deck under seismic excitations

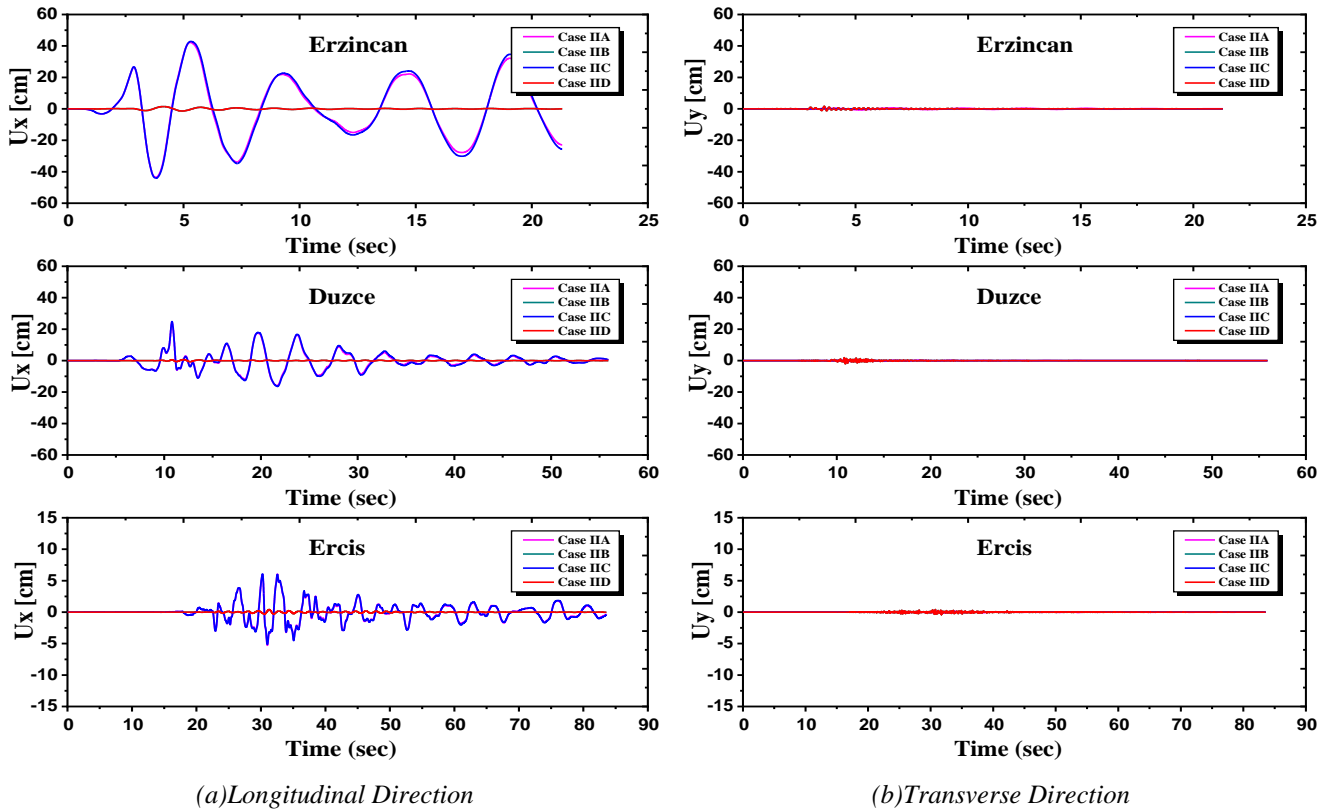


Fig. 14. Top pylon displacement under seismic excitations.

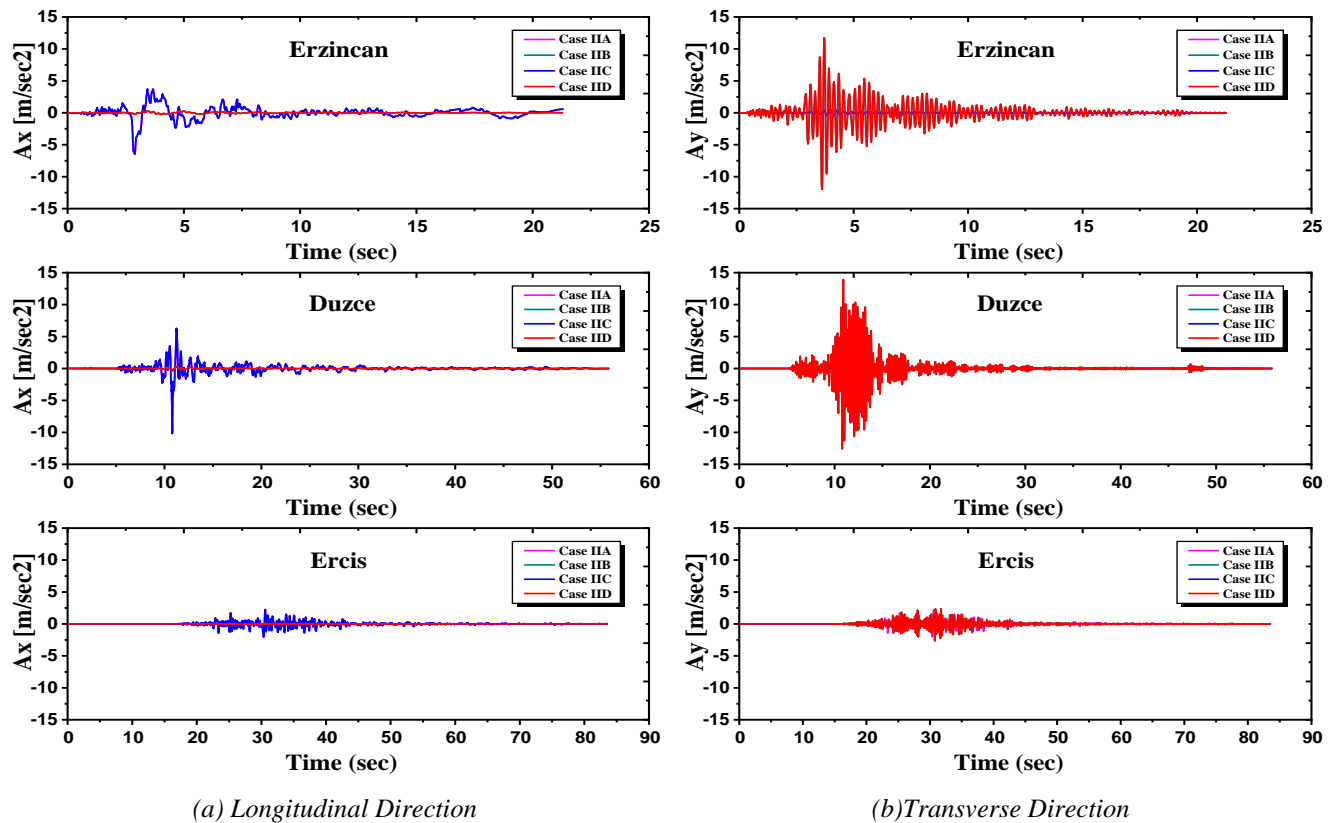


Fig. 15. Pylon acceleration under seismic excitations.

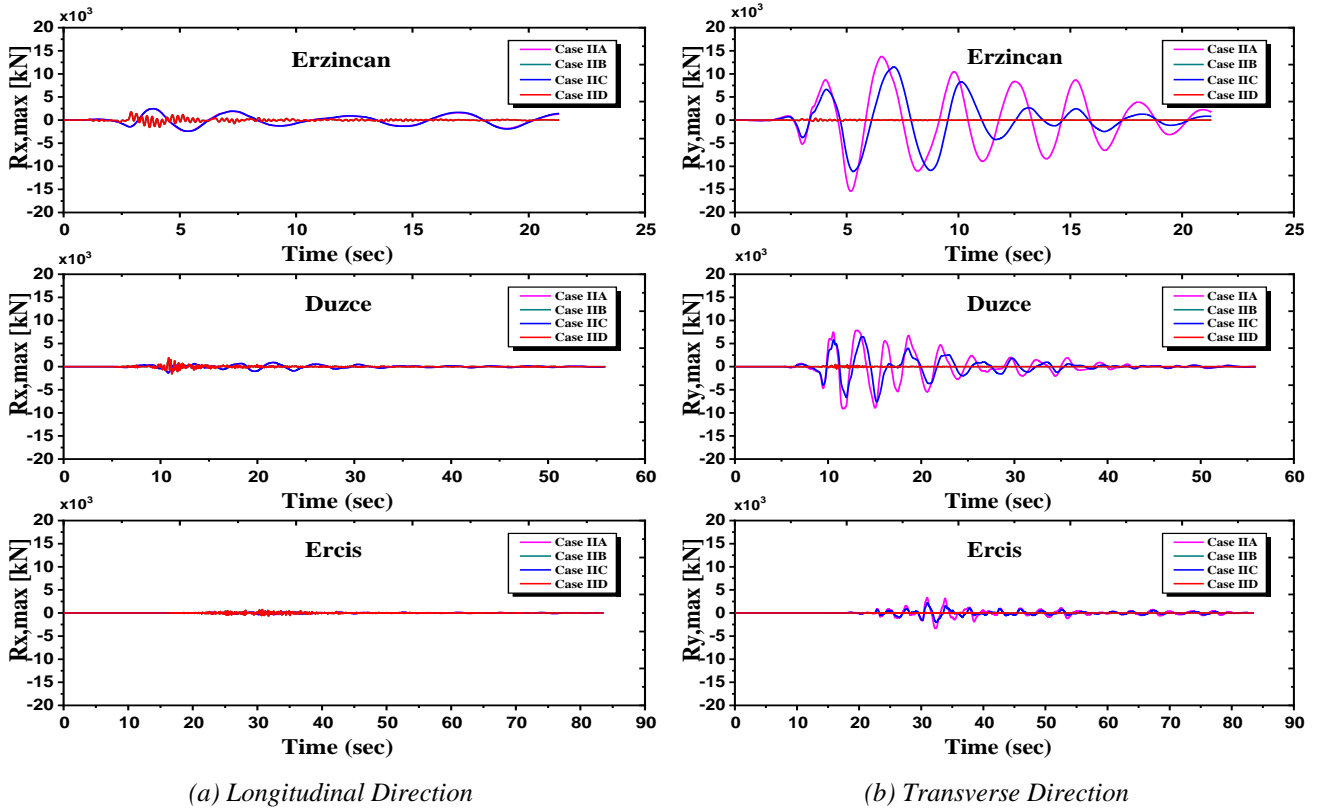


Fig. 16. Top pylon base shear under seismic excitations

Optimum location

Figs. 17-20 illustrate a comparison of peak values of $U_{z,max}$, U_x , U_y , $R_{x,max}$, $R_{y,max}$, A_x , and A_y responses for case (D) between the two groups (I&II) under seismic excitations. It is clear that case (IID) has the capacity to decrease the seismic response more effectively compared to case (ID). Case (IID) represents three SCFP isolators located between the deck and strut attached to the pylon only. On a practical note, it is difficult to apply the pylon isolation system in engineering practice due to potential overturning and instability of the central pylon.

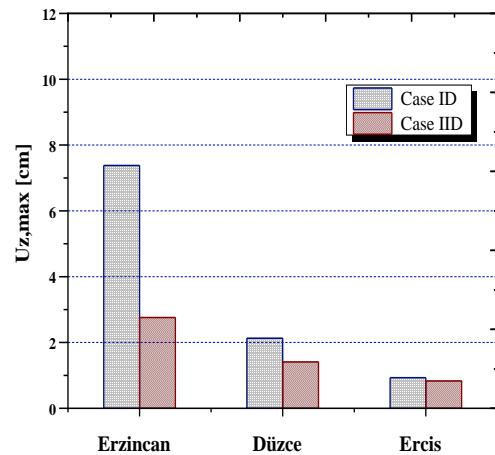


Fig. 17. Comparison between peak of maximum vertical displacement of the deck under seismic excitations

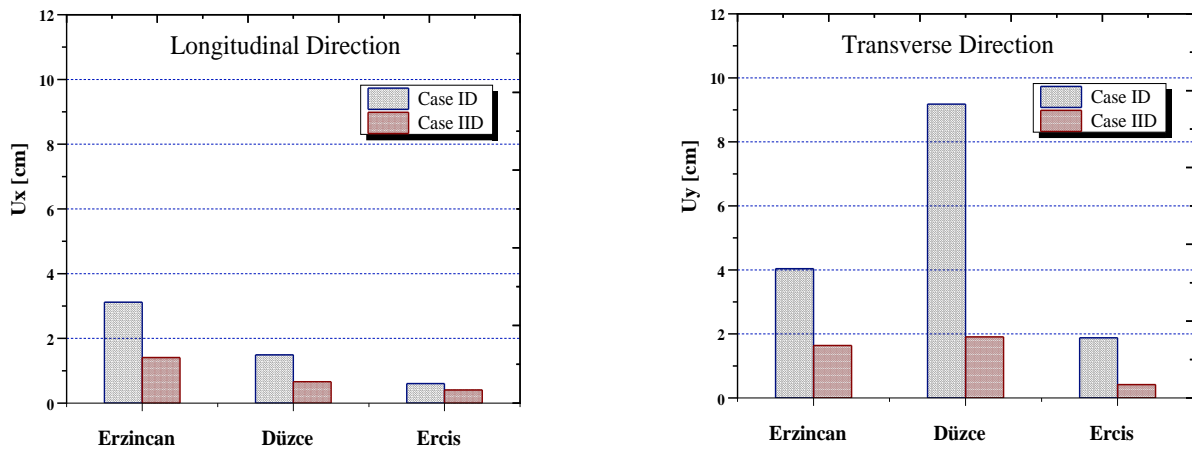


Fig. 18. Comparison between peak of top pylon displacement under seismic excitations.

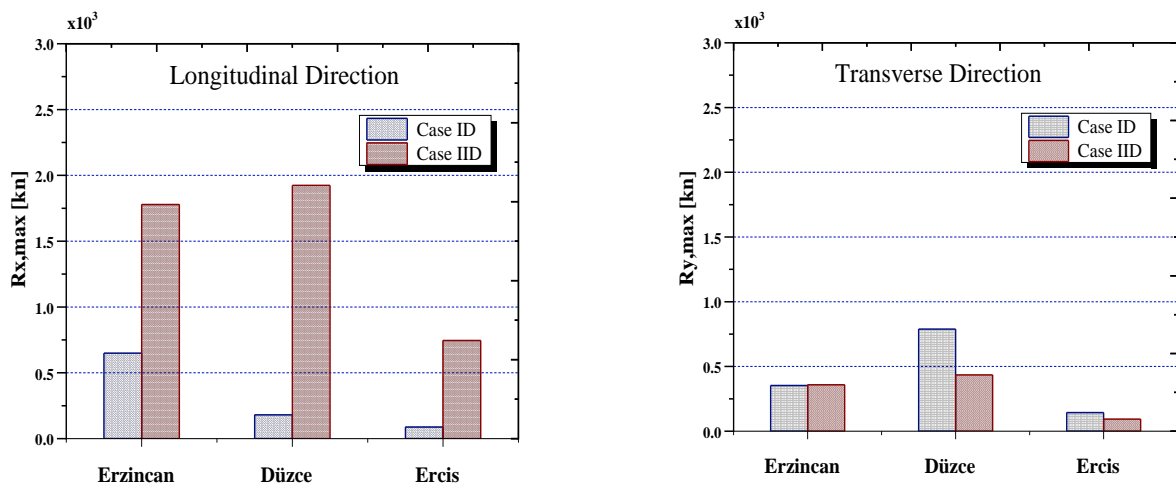


Fig. 19. Comparison between peak of maximum pylon base shear under seismic excitations.

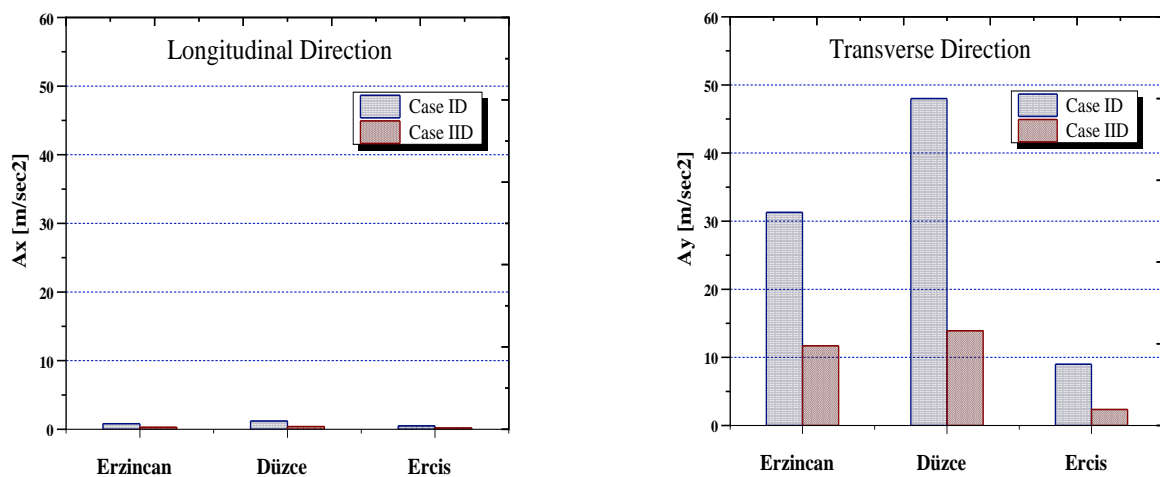


Fig. 20. Comparison between peak of top pylon acceleration under seismic excitations.

VII. SUMMARY AND CONCLUSION

The structural response of Manavgat cable-stayed bridge under seismic excitations has been studied to determine the optimum location of isolation devices (SCFP). Analytical measurements of the bridge responses were used to evaluate the performance of the bridge. The main response parameters considered were deck displacement, pylon base shear, top of pylon displacement, and top of pylon acceleration. A finite element model of the bridge was created, and its accuracy was verified using SAP2000. SCFP was applied to various locations of the bridge under three ground motions. The main conclusions of this study can be summarized as follows:

- I. The isolation system is effective in increasing periods of the bridge significantly, thus decreasing the internal reactions of the bridge.
- II. SCFP reduced the vertical displacement of the bridge deck, base shear, and displacement of the pylon significantly.
- III. The usage of isolation devices at end spans provides some benefits to the internal forces of the bridge. However, allowing the end spans to displace can lead to extensive damage due to pounding. Therefore, the absence of isolators at the end spans is safer and more effective.
- IV. The location of the isolation system between the pylon and foundation has shown some reduction in the strong axis bending demands of the superstructure. However, the isolation in this particular location is not sufficient to control the seismic bending demands on the superstructure. Finally, it is difficult to apply the pylon isolation system in engineering practice due to fear of overturning and instability of the central pylon.

REFERENCES

- [1] Datta T (1996) Control of dynamic response of structures. *Emerging Trends in Vibration and Noise Engineering*, 1, 101.
- [2] Rana R, Soong TT (1998) Parametric study and simplified design of tuned mass dampers. *Engineering structures*, 20(3), 193-204.
- [3] Ali HM, Abdel-Ghaffar AM (1995). Modeling the nonlinear seismic behavior of cable-stayed bridges with passive control bearings. *Computers & Structures*, 54(3), 461-492.
- [4] Ali HM, Abdel-Ghaffar AM (1994). Seismic energy dissipation for cable-stayed bridges using passive devices. *Earthquake engineering & structural dynamics*, 23(8), 877-893.
- [5] Constantinou MC, Reinhorn AM, Mokha A, Watson R (1991). Displacement control device for base-isolated bridges. *Earthquake Spectra*, 7(2), 179-200.
- [6] Constantinou MC, Kartoum A, Reinhorn AM, Bradford P (1992). Sliding isolation system for bridges: Experimental study. *Earthquake Spectra*, 8(3), 321-344.
- [7] Iemura H, Pradono MH (2002). Passive and semi-active seismic response control of a cable-stayed bridge. *Journal of Structural Control*, 9(3), 189-204.
- [8] Wesolowsky MJ, Wilson JC (2003). Seismic isolation of cable-stayed bridges for near-field ground motions. *Earthquake engineering & structural dynamics*, 32(13), 2107-2126.
- [9] Casciati F, Cimellaro GP, Domaneschi M (2008). Seismic reliability of a cable-stayed bridge retrofitted with hysteretic devices. *Computers & Structures*, 86(17-18), 1769-1781.
- [10] Soneji BB, Jangid RS (2006). Effectiveness of seismic isolation for cable-stayed bridges. *International Journal of Structural Stability and Dynamics*, 6(01), 77-96.
- [11] Xu Y, Wang R, Li J (2016). Experimental verification of a cable-stayed bridge model using passive energy dissipation devices. *Journal of Bridge Engineering*, 21(12), 04016092.
- [12] Soneji BB, Jangid RS (2007). Passive hybrid systems for earthquake protection of cable-stayed bridge. *Engineering structures*, 29(1), 57-70.
- [13] Casas J, Ismail M (2014). Novel isolation device for protection of cable-stayed bridges against near-fault earthquakes.
- [14] Ismail M, Rodellar J, Ikhoulane F (2010). An innovative isolation device for aseismic design. *Engineering Structures*, 32(4), 1168-1183.
- [15] Camara A, Astiz MA (2014) Analysis and control of cable-stayed bridges subject to seismic action. *Struct Eng Int*
- [16] Elkady AZ, Taylor T, Ansari F (2017) Lateral free vibration test of cable stayed bridges with tuned mass damper using structural health monitoring. *International Conference on Advances in Structural and Geotechnical Engineering*.
- [17] Elkady AZ, Seleemah MA, Ansari F (2018) Structural response of a cable-stayed bridge subjected to lateral seismic excitations. *Journal of Civil Structural Health Monitoring*, 8, 417-430.
- [18] Alshaer MF, Elkady AZ, Sakr MA, Seleemah A (2022) Enhancing Seismic Performance of Cable-Stayed Bridges using Tuned Mass Dampers. *Journal of Engineering Research*, 6(2), 45-49.
- [19] Calvi PM, Moratti M, Calvi GM (2016) Seismic isolation devices based on sliding between surfaces with variable friction coefficient. *Earthquake Spectra*, 32(4), 2291-2315.
- [20] Mostaghel N, Tanbakuchi J (1983) Response of sliding structures to earthquake support motion. *Earthquake engineering & structural dynamics*, 11(6), 729-748.
- [21] Zayas VA, Low SS, Mahin SA (1990) A simple pendulum technique for achieving seismic isolation. *Earthquake spectra*, 6(2), 317-333.
- [22] Mokha A, Constantinou M, Reinhorn A (1990) Teflon bearings in base isolation I: Testing. *Journal of Structural Engineering*, 116(2), 438-454.
- [23] Constantinou M, Mokha A, Reinhorn A (1990) Teflon bearings in base isolation II: Modeling. *Journal of Structural Engineering*, 116(2), 455-474.
- [24] Fenz DM, Constantinou MC (2008) Spherical sliding isolation bearings with adaptive behavior: Experimental verification. *Earthquake engineering & structural dynamics*, 37(2), 185-205.
- [25] Morgan TA, Mahin SA (2010) Achieving reliable seismic performance enhancement using multi-stage friction

This article can be downloaded from here: www.ijaems.com

57

©2023 The Author(s). Published by Infogain Publication, This work is licensed under a Creative Commons Attribution 4.0 License.

<http://creativecommons.org/licenses/by/4.0/>

- pendulum isolators. *Earthquake Engineering & Structural Dynamics*, 39(13), 1443-1461.
- [26] Tsai CS, Lin YC, Su HC (2010) Characterization and modeling of multiple friction pendulum isolation system with numerous sliding interfaces. *Earthquake engineering & structural dynamics*, 39(13), 1463-1491.
- [27] Han Q, Wen J, Du X, Zhong Z, Hao H (2018). Nonlinear seismic response of a base isolated single pylon cable-stayed bridge. *Engineering Structures*, 175, 806-821.
- [28] Fenz DM, Constantinou MC (2006). Behavior of the double concave friction pendulum bearing. *Earthquake engineering & structural dynamics*, 35(11), 1403-1424.
- [29] Fenz DM, Constantinou MC (2008). Modeling triple friction pendulum bearings for response-history analysis. *Earthquake Spectra*, 24(4), 1011-1028.
- [30] Sarlis AA, Constantinou MC (2016). A model of triple friction pendulum bearing for general geometric and frictional parameters. *Earthquake Engineering & Structural Dynamics*, 45(11), 1837-1853.
- [31] Lee D, Constantinou MC (2016). Quintuple friction pendulum isolator: behavior, modeling, and validation. *Earthquake Spectra*, 32(3), 1607-1626.
- [32] Tsopelas P, Constantinou MC, Kim YS, Okamoto S (1996). Experimental study of FPS system in bridge seismic isolation. *Earthquake Engineering & Structural Dynamics*, 25(1), 65-78.
- [33] Kim YS, Yun CB (2007). Seismic response characteristics of bridges using double concave friction pendulum bearings with tri-linear behavior. *Engineering Structures*, 29(11), 3082-3093.
- [34] Tsai CS, Lin YC, Chen WS, Chiang TC, Chen BJ (2010). Piecewise exact solution for seismic mitigation analysis of bridges equipped with sliding-type isolators. *Structural engineering and mechanics: An international journal*, 35(2), 205-215.
- [35] Soneji BB, Jangid RS (2006). Effectiveness of seismic isolation for cable-stayed bridges. *International Journal of Structural Stability and Dynamics*, 6(01), 77-96.
- [36] Chang KC, Mo YL, Chen CC, Lai LAC, Chou CC (2004). Lessons learned from the damaged Chi-Lu cable-stayed bridge. *Journal of Bridge Engineering*, 9(4), 343-352.
- [37] Chadwell CB (2003). Seismic response of single tower cable-stayed bridges. University of California, Berkeley.
- [38] Yoshikawa M, Hayashi H, Kawakita S, Hayashida M (2000). Construction of Benten Viaduct, rigid-frame bridge with seismic isolators at the foot of piers. *Cement and Concrete Composites*, 22(1), 39-46.
- [39] Ates S, Constantinou MC (2011). Example of application of response spectrum analysis for seismically isolated curved bridges including soil-foundation effects. *Soil Dynamics and Earthquake Engineering*, 31(4), 648-661.
- [40] Atmaca B, Yurdakul M, Ateş Ş (2014). Nonlinear dynamic analysis of base isolated cable-stayed bridge under earthquake excitations. *Soil Dynamics and Earthquake Engineering*, 66, 314-318.
- [41] Javanmardi A, Ibrahim Z, Ghaedi K, Jameel M, Khatibi H, Suhatri M (2017). Seismic response characteristics of a base isolated cable-stayed bridge under moderate and strong ground motions. *Archives of Civil and Mechanical Engineering*, 17, 419-432.
- [42] Kanok-Nukulchai W, Yiu PKA, Brotton DM (1992). Mathematical modelling of cable-stayed bridges. *Structural Engineering International*, 2(2), 108-113.
- [43] Gambhir ML, de V. Batchelor B (1977). A finite element for 3-D prestressed cablenets. *International Journal for Numerical Methods in Engineering*, 11(11), 1699-1718.
- [44] Ozdemir H (1979). A finite element approach for cable problems. *International Journal of Solids and Structures*, 15(5), 427-437.
- [45] Karoumi R (1999). Some modeling aspects in the nonlinear finite element analysis of cable supported bridges. *Computers & Structures*, 71(4), 397-412.
- [46] Freire AMS, Negrao JHO, Lopes AV (2006). Geometrical nonlinearities on the static analysis of highly flexible steel cable-stayed bridges. *Computers & Structures*, 84(31-32), 2128-2140.
- [47] Ernst H, (1965). Der E-modul von seilenunterbercksichtigung des durchhanges. *Bauingenieur*, 40.
- [48] Wilson JC, Gravelle W (1991). Modelling of a cable-stayed bridge for dynamic analysis. *Earthquake Engineering & Structural Dynamics*, 20(8), 707-721.
- [49] Yoshikawa M, Hayashi H, Kawakita S, Hayashida M (2000). Construction of Benten Viaduct, rigid-frame bridge with seismic isolators at the foot of piers. *Cement and Concrete Composites*, 22(1), 39-46.
- [50] Ates S, Constantinou MC (2011). Example of application of response spectrum analysis for seismically isolated curved bridges including soil-foundation effects. *Soil Dynamics and Earthquake Engineering*, 31(4), 648-661.
- [51] Mosqueda G, Whittaker AS, Fenves GL, Mahin SA (2004). Experimental and analytical studies of the friction pendulum system for the seismic protection of simple bridges. *EERC 2004*, 1.
- [52] Oh ST, Kim YS (1998). Experimental and analytical investigation of a seismically isolated bridge model with friction pendulum system. *KSCE Journal of Civil Engineering*, 2, 265-272.
- [53] Pacific Earthquake Engineering Research Center (PEER). Web-Based PEER Ground Motion Database (Beta Version) [Interactive web-site database]. Berkeley, California (2010). http://peer.berkeley.edu/peer_ground_motion_database